Nonlinear Reduced Order Model of Rectangular High Aspect Ratio Wing with and without Follower Force Effects

Open Access

Norzaima Nordin[1,2], Thinesh Chandrasegaran[1], Mohammad Yazdi Harmin[1,*]

[1] Department of Aerospace Engineering, Faculty of Engineering, Universiti Putra Malaysia, 43400 Serdang, Selangor, Malaysia
[2] Department of Aeronautical Engineering and Aviation, Faculty of Engineering, Universiti Pertahanan Nasional Malaysia, 57000 Sungai Besi, Kuala Lumpur, Malaysia

ARTICLE INFO	ABSTRACT
	This paper describes a technique proposed to characterized the nonlinear properties of the High Aspect Ratio (HAR) wing model by developing a Nonlinear Reduced Order Model (NROM) via Combined Modal/Finite Element (CMFE) approach. In this study, nonlinear static analysis of HAR wing model under non-follower and follower forces was performed through the Finite Element Method (FEM) using MSC NASTRAN software. Three types of loading (uniform loading, twist loading and leading edge loading) are considered in order to demonstrate the bending and twisting deformations including a combination of bending-twisting deformation for both non-follower and follower force effects. For verification, the accuracy of the developed NROM is presented in the form of mean error and its corresponding standard deviation against the conventional FEM of nonlinear static analysis. It was found that the developed NROM via CMFE approach had shown a good accuracy compared to FEM analysis with a significant saving in computational time. Another finding shows that the NROM by combining uniform and twist loading cases can sufficiently predict the leading edge case; hence provide a possibility to predict the nonlinear aerostatic behaviour. Besides that, comparison for the load case under non-follower and follower force effects are also demonstrated. The results show that the inclusion of the follower force effect indicates a greater deflection than the system of non-follower force for all the considered load cases.

1. Introduction

The demand for the next generation of aircraft design is mainly focused on fuel efficiency and the ability to endure long missions. Most of the modern jet engine aircraft are using fossil fuels to produce required thrust, which leads to the production of carbon dioxide (CO_2) and other greenhouse gasses that warm the environment. To compensate the issue, researchers have been exploring the advantages of the High Aspect Ratio (HAR) wing design as its ability to improve fuel efficiency and flight endurance performance. This is mainly due to the fact that HAR wings could

---

* Corresponding author.
E-mail address: myazdi@upm.edu.my (Mohammad Yazdi Harmin)

effectively provide an aircraft with a higher lift to drag ratio [1]. It can be seen through the equations for the total drag coefficient can thus be written as:

$$C_D = C_{D0} + C_{Di} = C_{D0} + \frac{(C_L)^2}{\pi.e'.AR} \qquad (1)$$

where C_{D0}, C_{Di}, C_L, e' and AR are the profile drag coefficient, induced drag coefficient, lift coefficient, span efficiency factor and aspect ratio of the wing, respectively. This equation showing that the induced drag which is principally due to wing tip or trailing edge vortices will decrease by increasing the aspect ratio of the wing.

However, despite aforementioned significant advantageous from HAR wing design, most of the researchers are still have to work on the optimization of its application because of its structural design, which originates a geometrical nonlinear issue. The design of the HAR wing considered as not yet matured because of limited understanding on the geometric nonlinear aeroelastic behavior of HAR wing. This is due to the flexibility issue that had exhibited larger deformation under the same flight condition [2]. This reflects the changes in dynamic behavior and in aeroelastic response, resulting in instabilities [3, 4]. Therefore, it is important to take into account geometric nonlinearities in the design of HAR wings, as well as to generate an accurate computational codes which couple the aerodynamic and structural models in the presence of nonlinearities.

Geometrical nonlinearity on HAR wing is caused by the large displacement and the effect of continuous acting aerodynamic forces [5-7]. Moreover, to better understand on geometrical nonlinearity behavior, one must also to clarify the consequence of considering conservative forces of Non-Follower Force (NFF) and non-conservative forces of Follower Force (FF) for the accuracy on the aerodynamic-structural analysis. In reality, the direction of the force will change with deformation of the wing due to the nature of the actual aerodynamic. This will be referred as FF. To date, there has been little work published in the literature of FF consideration on the geometrical effect of the HAR wing structure [8]. Kim *et al.,* had conducted an experimental study to compare static response data of qualification test article collected for the cases of FF and NFF.

In the experiment, a FF setup was built to provide realistic loads as in the actual aircraft wings. The study had shown that analysis with FF exhibited larger deformation compared to analysis with NFF [9]. Xie *et al.,* have made a comparison study between linear and nonlinear and validate with wind tunnel test result in static aeroelastic analysis. One of the findings has stated that in the nonlinear analysis, the aerosurface is automatically updated with structural deflection and the deflection is mainly caused by FF effect [10]. Castellani *et al.,* had used two methods which are based on nonlinear Finite Element Method (FEM) and on multibody dynamic to predict nonlinear static aeroelasticity based on non-follower and follower force effects [11]. 20% of increment different in term of tip deformation was observed on FF over NFF. These studies highlighted the significance of FF inclusion on the geometrically nonlinear analysis of HAR wing, which has been neglected conventionally.

Research has shown that a lot of methods that was published on the geometrical nonlinearity analysis. Nonlinear FEM is commonly used to calculate the stiffness and displacement of a model subjected to aeroelastic analysis. However, it requires expensive computation Newton Raphson and needs high computational time. Previous study has successfully shown that Nonlinear Reduced Order Model (NROM) method is able to compensate computational time by reducing the scale of the problem, thus analyze the characteristics of large HAR wing geometrics nonlinearity easily [10]. This offers a better computational method for complex structural analysis and potential for nearly real time analysis. In other work, McEwan *et al.,* propose Combined Modal/Finite Element (CMFE) method by static analysis with numbers of specified static load cases [12]. The displacement results

were then curve fitted using regression analysis to show the nonlinear stiffness values, which reflect structural nonlinear characteristics in structural motion equations. Harmin and Cooper extended this method by implied the CMFE approach for modeling the geometric nonlinearity of a large aspect ratio wing model. This approach was used to predict the static deflection, gust response and limit cycle oscillation [4]. However, it was limited to NFF analysis condition. In 2018, Thinesh and Harmin conducted a NROM analysis using the CMFE approach on a wing plate model with NFF consideration [13]. The study shows the significance of the selection of modes and test cases in the accuracy of the NROM.

The focus of the present investigation is on extending the recent success obtained of NROM via CMFE of HAR rectangular wing plate, see [13] with the inclusion of the follower forces effect. To this end, a comparison study of FEM between non-follower and follower forces will be made. The validation of the accuracy of NROM via CMFE approach with FEM of nonlinear properties of the HAR wing model at different types of loading will be performed.

2. Simulation Model
2.1 HAR Wing Model

A HAR wing model is simulated in order to validate the accuracy of NROM and to complete the static analysis on geometric nonlinearity. The HAR wing simulation model is constructed by 16 sections based on Rosly N.A [14] as depicted in Figure 1. A total of 17 ribs were equally divided along the leading and trailing spars. The total wing span length is denoted as L_S, while the distance between the rib is denoted as L_R. The geometric and material properties of HAR wing model are summarized in Table 1.
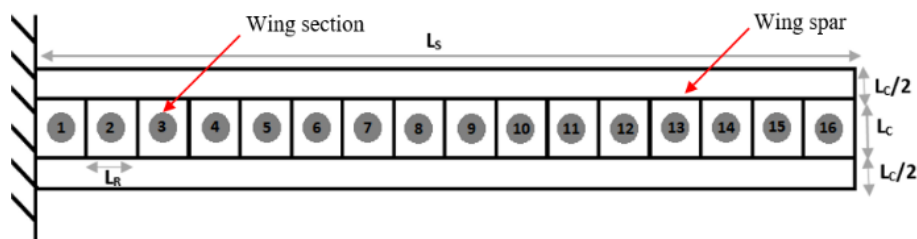
Fig. 1. Layout of HAR wing model (L_S = span length, L_C = plate chord length, L_R = rib length)

Table 1
Design parameters of the HAR wing model

Material and geometric properties of HAR wing	
Span length, L_S	0.8 m
Plate chord length, L_C	0.025 m
Density of spring steel-plate, ρ_{ss}	7833.413 kgm^{-3}
Poisson's ratio of spring steel-plate, υ_{ss}	0.295

Though the existence of lateral deformation of the HAR wing model in geometric nonlinear static analysis, two types of modes were taken into account for the establishment of NROM and to evaluate the accuracy. Two modes are used in the establishment of NROM is depicted in Table 2.

Table 2
Modes in the establishment of NROM

Mode	Type of modes	Eigenvalues
1	1st bending	90.4111
6	1st torsion	256100.6

2.2 Nonlinear Finite Element Method

A procedure for the linear and nonlinear static analysis based on linear and nonlinear static finite element analysis in MSC NASTRAN (SOL 101 and SOL 106) was performed on the HAR wing model at the different condition of the load applied. Each case will have considered for both non-follower and follower forces. In the follower forces analysis, the main parameter needs to be considered is the direction of the force itself. The force needs to be parallel to the cross product vector from G1 to G2 and G3 to G4 which identified in MSC NASTRAN bulk data [15] with large displacement (LGDISP) consideration.

2.3 Nonlinear ROM via CMFE Approach

Using the CMFE [4, 12] approach, the NROM is developed with respect to the characteristics of the prescribed load cases for the nonlinear static solution. A linear static analysis is also to be conducted to verify the degree of nonlinearities of the HAR wing plate model for the pre-defined load cases. A normal mode analysis is done in order to identify the corresponding eigensolutions (eigenvalue and eigenvector) and to determine the characteristics of each mode. The nonlinear force-displacement relationship for the prescribed load cases is utilized to evaluate the nonlinear stiffness terms using through curve fitting. The nonlinear stiffness term is to be added to the linear equation of motion in modal space to characterize the equation of motion with geometric nonlinearity. The NROM which is the equation of motion characterized with the nonlinear stiffness term is then used to predict the deflection for a defined force input in modal space. The predicted deflection is then converted to the physical space coordinate to be verified with the conventional FEA results of nonlinear static solutions.

The static system equation refers to (2), based on the mathematical modelling used by Harmin *et al.,* [4], where $[E_L]$ is assembled linear stiffness matrices of size NR × NR; $\{F\}$ is the NR × 1 applied modal force; $\{E_{NL}(p)\}$ is a polynomial form as the product of Nth order modal displacements multiplied by the unknown nonlinear stiffness coefficients and p is the modal displacement.

$$[E_L]\{p\} + \{E_{NL}(p)\} = \{F\} \tag{2}$$

It is to be noted that the left-hand side of the static system equation is the stiffness restoring forces which compromises of the linear and nonlinear stiffness. By rearranging (2), it is obtained

$$\{F\} - [E_L]\{p\} = \{E_{NL}(p)\} \tag{3}$$

From the equations above, let

$$[D] = [\{F\} - [E_L]\{p\}] \tag{4}$$

where D is 1 × NL vector; NL is the number of load cases considered for the investigation. Since $\{E_{NL}(p)\}$ is a polynomial function hence the matrix is split into

$$\{E_{NL}(p)\} = \begin{bmatrix} p^2 & p^3 & \cdots \end{bmatrix} \begin{bmatrix} A_1 \\ A_2 \\ \vdots \end{bmatrix} \tag{5}$$

where A_1 and A_2 are the constants in the polynomial equation. The polynomial constants can be determined by

$$\begin{bmatrix} A_1 \\ A_2 \\ \vdots \end{bmatrix} = [D]\ [\text{p}^2\ \text{p}^3\ ...]^{\text{inv}} \tag{6}$$

where $[\text{p}^2\ \text{p}^3 \cdots]^{\text{inv}}$ is the pseudo-inverse of the $\begin{bmatrix} p^2 & p^3 & \cdots \end{bmatrix}$ matrix. Once the coefficients of the polynomial are to determined, the NROM equations can then be formed. A Newton Raphson method analysis is employed on the NROM equation in order to find the modal displacement for a defined force. The modal force can be obtained by refer to Eq. (7) with ψ is N × NR matrix of the underlying linear mode shapes of the selected mode while the physical displacement, x can be obtained by refer to Eq. (8).

$$\{F\} = [\psi]\ \{\mathbb{F}\} \tag{7}$$

$$[x] = [\psi]\ [p] \tag{8}$$

To verify the accuracy of the NROM with the conventional FEA analysis, the mean and standard deviation of the error for each analysis are calculated and displayed graphically; where the error is the differences between the solution obtained by NROM and FEA of the nonlinear static solution.

2.4 Strategy Generating Load Cases

The rationality of the load cases selection significantly affected the accuracy of nonlinear stiffness coefficient in nonlinear ROM. The selection of load cases must meet certain conditions which are; (a) the selected load cases must be able to capture the linear and nonlinear region of deformations and (b) the selected load cases must be rational and interested in the research (e.g. the deformation must be less than 0.4 m to meet the safety margin of wind tunnel test section). To do so, present study consider three condition of loading in order to demonstrate the bending and twisting deformation under non-follower and follower forces state, which are; (a) uniformly distributed loading over the entire HAR wing spar model to define bending profile, (b) uniformly distributed loading along leading and trailing edge spar with one of the loading opposite load direction to capture twist profile and (c) uniformly distributed loading over leading edge of the HAR wing spar model which including both deformations profile.

2.4.1 Uniform loading

The first load case is to generate a bending profile of the HAR wing plate. For this case, the HAR wing spar is subjected to a distributed load from the wing root to the wing tip as shown in Figure 2. The distributed load is uniformly applied to range from 0.003N to 0.0015N.
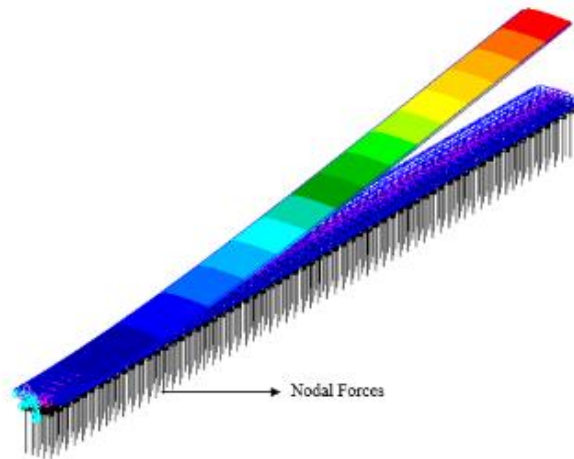
Fig. 2. Uniform loading distribution on HAR wing plate model

2.4.2 Twist loading

The second load case is to capture the rotational profile of the HAR wing model. For this case, nodal forces on each node of the leading edge and trailing edge of HAR wing spar is subjected to a uniform distributed load with the same magnitude but in the opposite direction. Figure 3 shows the rotation of the HAR wing model with a load ranging from 0.2N to 1N.
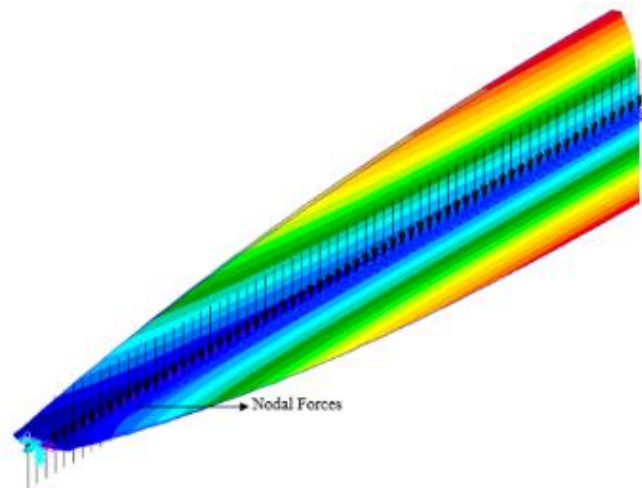
Fig. 3. Uniform loading distribution on the leading edge and trailing edge of the HAR wing plate model

2.4.3 Leading edge loading

The third load case is to simulate aerostatic load circumstances. For symmetrical airfoils, the aerodynamic center of an airfoil is located approximately 25% of the airfoil. Hence, for this HAR wing is generalized to be point concentrated with aerodynamic loading on the wing plate. For this case, each node on the leading edge of the HAR wing spar is subjected to a uniform distributed load in order to replicate an aerostatic load. Figure 4 shows the leading edge loading of the HAR wing model with load range from 0.015N to 0.075N.
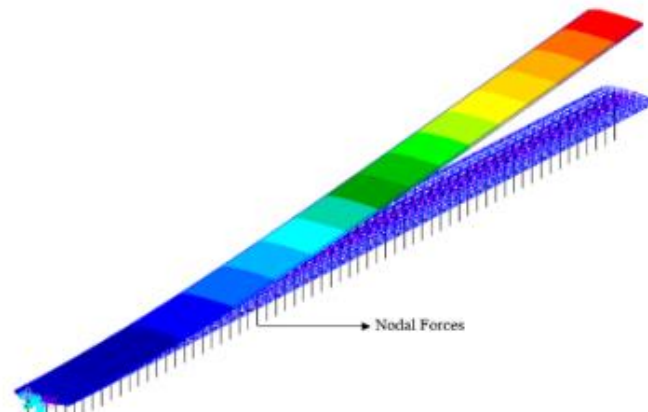
Fig. 4. Uniform loading distribution on the leading edge of the HAR wing plate model

3. Results and Discussions

3.1 Numerical Results of Non-Follower and Follower Forces

The results are presented into three different types of analysis approaches, which are linear, nonlinear non-follower forces and nonlinear with follower forces analysis. Figure 5 shows the deformation of the wing tip subjected to three different load condition with consideration for both non-follower and follower force effects. In general, it was observed that the wing structure had experienced a stiffness hardening effect, occurred as the tip of the wing is deflected beyond a certain limit. For all load cases, it can be seen that the follower force effects act to stiffen the structure with a much lower order of hardening effect compare to the nonlinear follower forces. The results are valid with the definition of follower forces where the force remains normal to the surface deflection, thus the concentration of the force to the corresponding structural grid will always be at the highest magnitude. Obviously, this will result in a greater deflection than the system of a non-follower force.
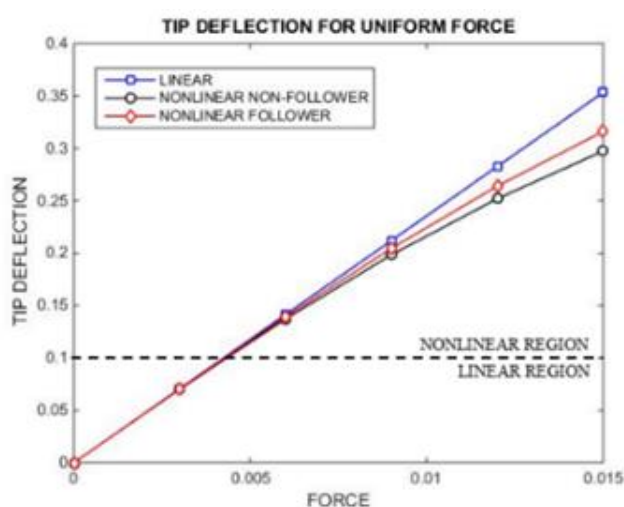
(a) Tip bending deformation for uniform loading
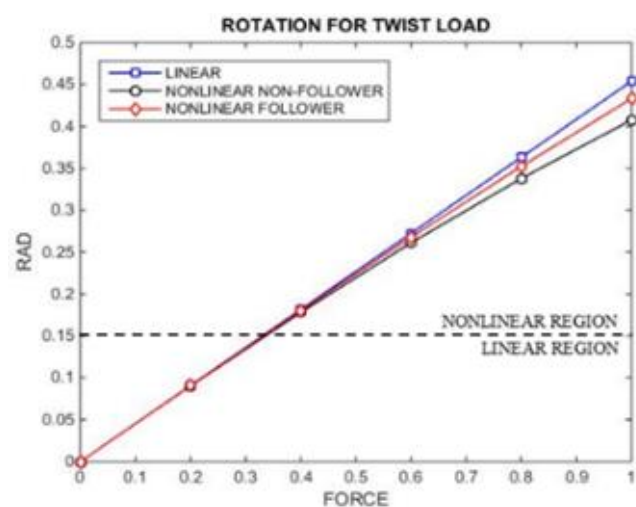
(b) Tip twisting deformation for twist loading
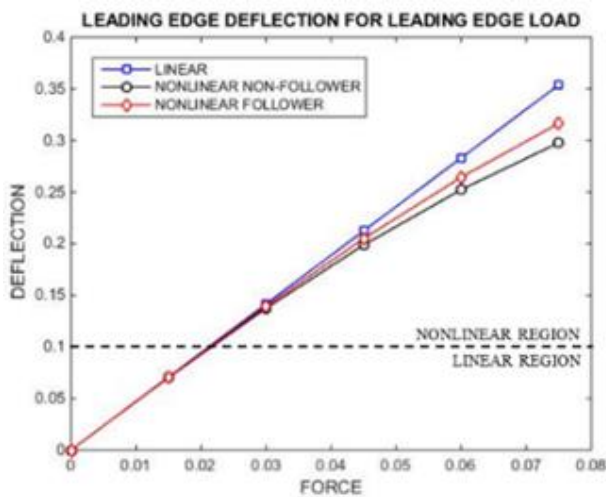
(c) Tip bending deformation at the leading edge
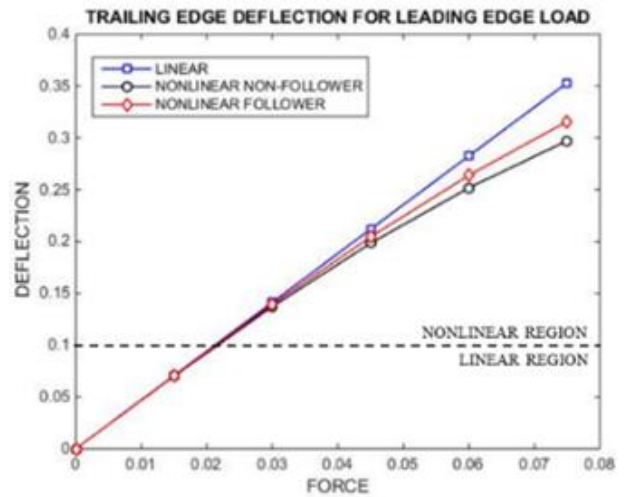
(d) Tip bending deformation at trailing edge
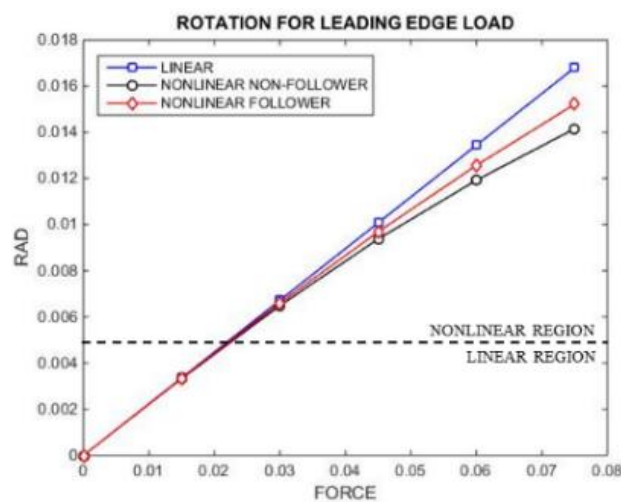
(e) Tip twisting deformations

Fig. 5. Tip deformation for linear and nonlinear non-follower and follower forces

Table 3 represents the relative difference of maximum tip deformation between the nonlinear follower and follower force for all type of load cases.

Table 3
Relative percentage difference at different type of loads

Type of load	Force	Deformation	The relative difference (nonlinear NFF and nonlinear FF)
Uniform	0.015 N	Tip bending	6.25%
Twist	1.000 N	Tip twisting	5.88%
		Tip bending at LE	6.28%
Leading edge	0.075 N	Tip bending at TE	6.26%
		Tip twisting	14.29%

3.2 Verification of NROM via CMFE Approach

The accuracy of the estimated NROM via CMFE approach is validated thru the comparison of the calculation results between NROM and Finite Element nonlinear static analysis for both non-follower and follower force effect. NROM is obtained by CMFE from the load cases and the corresponding

deformations, so the nonlinear structural equation must fit the result of all sets of test load cases and the corresponding linear and nonlinear deformations. More importantly, the nonlinear structure equation should fit the load cases and their corresponding deformations, having good adaptability in the calculation to predict different forms of loads. Table 4 presents the detail of three sets of different cases to validate with NROM via CMFE approach. All details investigation is discussed in the next section.

Table 4
Case identification

Case	Detail of NROM investigation	
	Type of load	Normal mode
1	Leading edge load	1st bending mode
		1st torsion mode
2	Uniform load	1st bending mode
	Twist Load	1st torsion mode
3	Uniform load	1st bending mode
	Twist Load	1st torsion mode
	Leading edge load	

3.3 Case 1 to Predict Deformations due to Uniform, Twist and Leading Edge Load

The NROM equations of Case 1 due to leading edge loading is presented in Table 5 (F_{b1} = Modal Force of 1st Bending Mode, F_{t1} = Modal Force of 1st Torsion Mode, P_{b1} = Modal Displacement of 1st Bending Mode, F_{t1} = Modal Displacement of 1st Torsion Mode) comparing between NROM model and FEM nonlinear static analysis.

Table 5
NROM equations

NROM equations	
Non-follower forces	$F_{B1} = 90.4\,P_{B1} + 64.91\,P_{B1}^2 + (3.777 \times 10^3)\,P_{B1}^3$
	$F_{T1} = 256100\,P_{T1} + (7.41 \times 10^8)\,P_{T1}^2 + (4.8 \times 10^{11})\,P_{T1}$
Follower forces	$F_{B1} = 90.4\,P_{B1} + 54.38\,P_{B1}^2 + (2.3 \times 10^3)\,P_{B1}^3$
	$F_{T1} = 256100\,P_{T1} + (7.0 \times 10^8)\,P_{T1}^2 + (4.3 \times 10^{11})\,P_{T1}^3$

3.3.1 NROM (case 1) to predict uniform loading

Figure 6 presents the summary result of mean error and standard deviation for both non-follower and follower force effect between NROM and FEM analysis. The result shows that the maximum mean error is found at the highest magnitude force with maximum mean error of approximately 4 mm for both cases. The results indicate the leading edge deformations used to construct the NROM is sufficiently adequate to predict the deformation of the HAR wing model due to uniform loading. The leading edge deformations are characterized with sufficient pure bending properties which contribute immensely to the accuracy of the NROM. The test cases selected for the construction of NROM also have a good constitution of linear and nonlinear properties for both non-follower and follower forces effect hence resulting in accurate NROM of the HAR wing model to predict the deformations due to uniform loading.
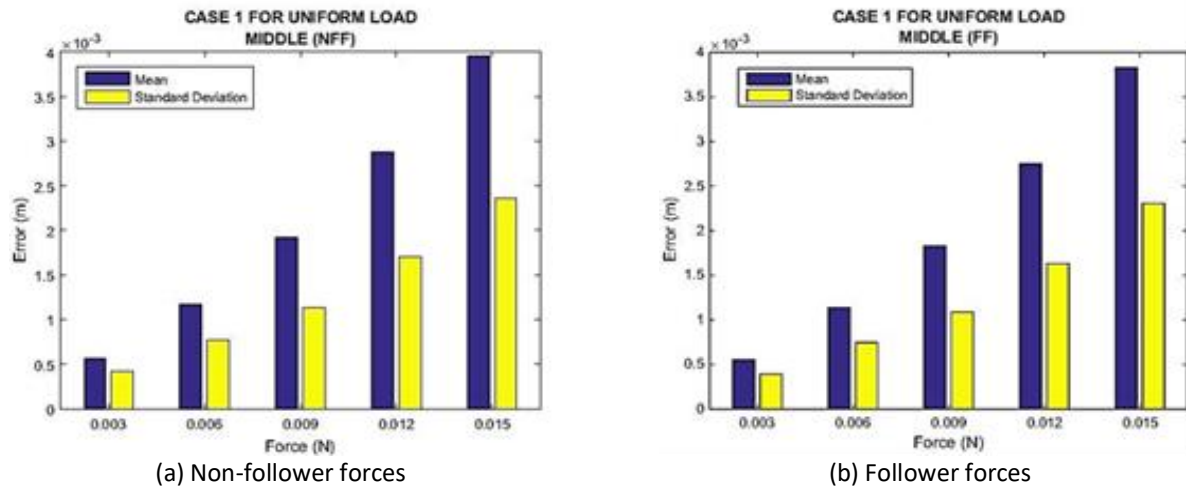
(a) Non-follower forces   (b) Follower forces
Fig. 6. Mean error and standard deviation of Case 1 for uniform loading

Overall, the NROM was able to predict the deformation of the HAR wing model with significant accuracy since the percentage of error relative to the wingspan of the HAR wing model is 0.5%.

3.3.2 NROM (case 1) to predict twist loading

Figure 7 presents the summary of mean error and standard deviation for both non-follower and follower force effect. Based on the results for both cases, the maximum mean error is found at the highest magnitude force with approximately maximum mean error 0.23 rad for both cases. The NROM equations are not able to predict the twist deformations based on the high mean error between the constructed NROM and FEM analysis. The NROM is not characterized with high rotational properties in order to predict the twist deformations since the test cases used in order to develop the NROM have relatively low twist deformations in comparison deformation due to leading edge load.
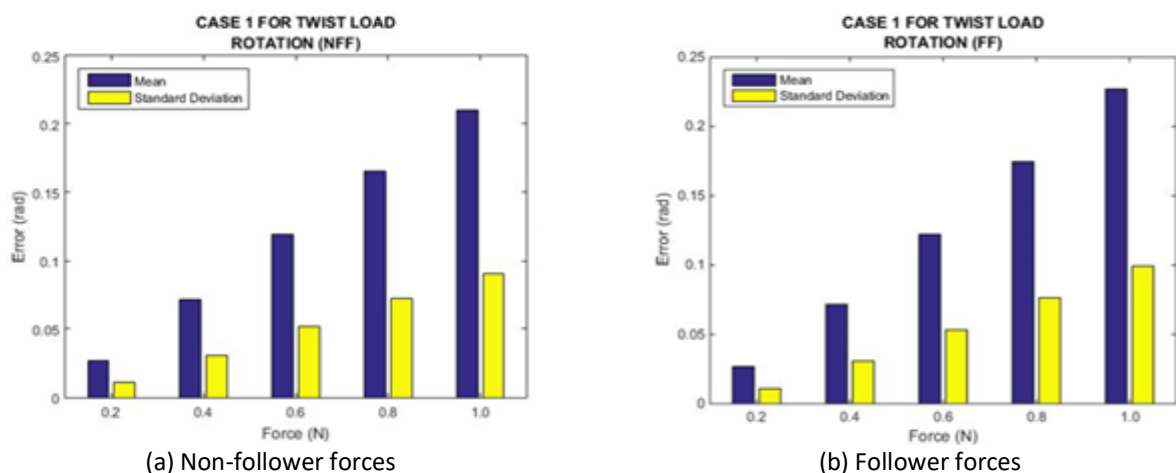
(a) Non-follower forces   (b) Follower forces
Fig. 7. Mean error and standard deviation of Case 1 for twist loading

3.3.3 NROM (case 1) to predict leading edge loading

Figure 8 presents the summary result of mean error and standard deviation for both non-follower and follower force effect to predict leading edge loading. Based on the results for both cases, all cases

show that the maximum mean error is found at the highest magnitude force with a maximum mean error of approximately 4 mm, 4 mm and 0.0008 rad for leading edge deformation, trailing edge deformation and rotation respectively.

(a) Leading edge

(b) Trailing edge

(c) Rotation
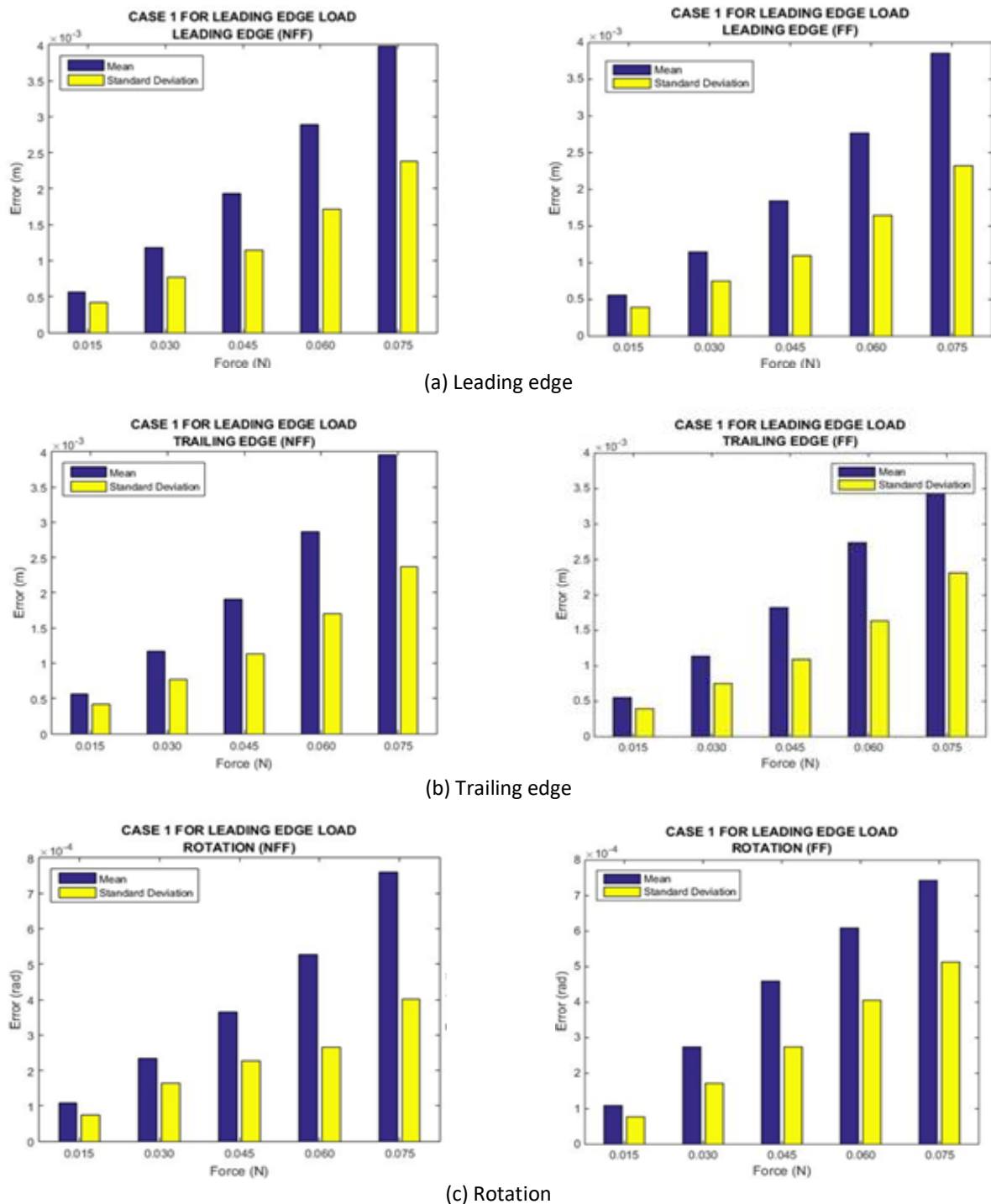
Fig. 8. Mean error and standard deviation of Case 1 for non-follower and follower forces for leading edge loading

Overall, the test cases used to develop the NROM are able to predict the deformation of the HAR wing model due to leading edge load even though these deformations have a combination of bending and twist deformation.

3.4 Case 2 to Predict Deformations due to Uniform, Twist and Leading Edge Load

The NROM equations of Case 2 including with uniform loading to capture bending profile and twist loading to capture rotational profile presented in Table 6.

Table 6
NROM equations

NROM equations	
Non-follower forces	$F_{B1} = 90.4\ P_{B1} + 64.92\ P_{B1}^2 + (3.77 \times 10^3)\ P_{B1}^3$
	$F_{T1} = 256100\ P_{T1} - (1.5 \times 10^6)\ P_{T1}^2 + (1.84 \times 10^{10})\ P_{T1}^3$
Follower forces	$F_{B1} = 90.4\ P_{B1} + 54.38\ P_{B1}^2 + (2.3 \times 10^3)\ P_{B1}^3$
	$F_{T1} = 256100\ P_{T1} + (1.2 \times 10^5)\ P_{T1}^2 + (5.9 \times 10^9)\ P_{T1}^3$

3.4.1 NROM (case 2) to predict uniform loading

Figure 9 portrays the summary result of mean error and standard deviation for both non-follower and follower force effect for the NROM case 2 to predict uniform loading deformations. Based on the results for both cases, the maximum mean error is found at the highest magnitude force with approximately maximum mean error 4 mm for both cases. The low mean error concludes the effectiveness of the NROM to predict the uniform loading deformation for the HAR wing model. The NROM which was developed with a combination of sufficient uniform loading and twist loading deformation enabling it to be excellent tool to predict uniform loading deformation.
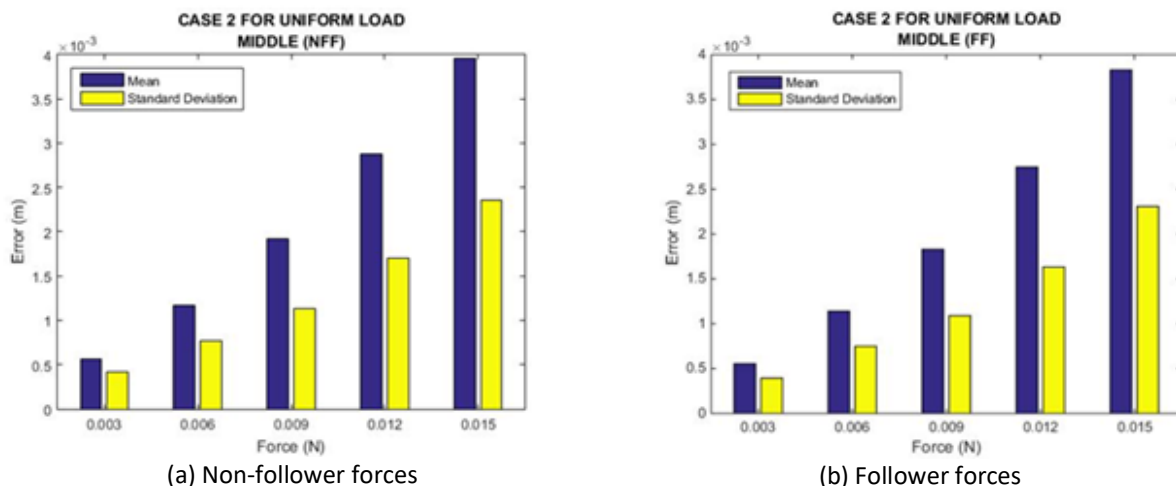
(a) Non-follower forces   (b) Follower forces
Fig. 9. Mean error and standard deviation of Case 2 for uniform loading

3.4.2 NROM (case 2) to predict twist loading

Figure 10 presents the summary result of mean error and standard deviation for both non-follower and follower force effect for the NROM case 2 to predict twist loading deformations. Based on the results for both cases, the maximum mean error is found at the highest magnitude force with approximately maximum mean error 0.016 rad for both cases. Since the NROM was equipped with sufficient twist deformation characteristics, the NROM was able to predict the twist deformation with significant accuracy. The NROM for case 2 also shows higher accuracy in prediction of twist deformation of NROM for case 1 which indicates the significance of including sufficient load cases in order to predict the desired cases and their deformation.

(a) Non-follower forces　　　　　　　　　　(b) Follower forces
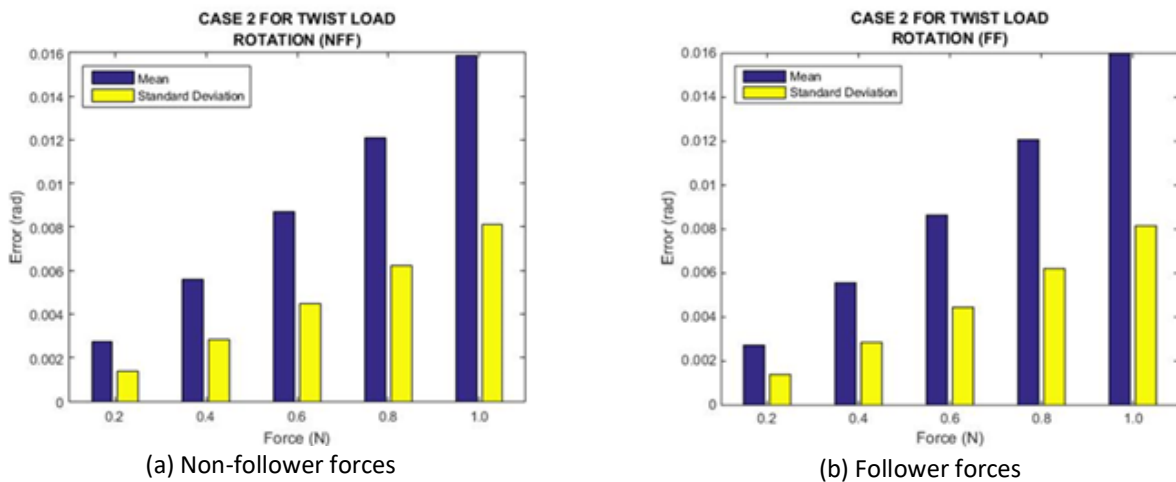
Fig. 10. Mean error and standard deviation of Case 2 for twist loading

3.4.3 NROM (case 2) to predict leading edge loading

Figure 11 presents the summary result of mean error and standard deviation for both non-follower and follower force effect for the NROM case 2 to predict leading edge loading. Based on the results for both cases, for leading and trailing edge deformation show that the maximum mean error is found at the highest magnitude force with approximately maximum mean error 4 mm for both cases. Meanwhile, for rotation, the error for the non-follower and follower force effect are 0.0018 rad and 0.0012 rad, respectively. The NROM for case 2 proves the combination of uniform loading deformation and twist loading deformation is sufficient to characterize and develop a NROM to predict the deformation of leading edge loading.

(a) Leading edge

(b) Trailing edge

(c) Rotation
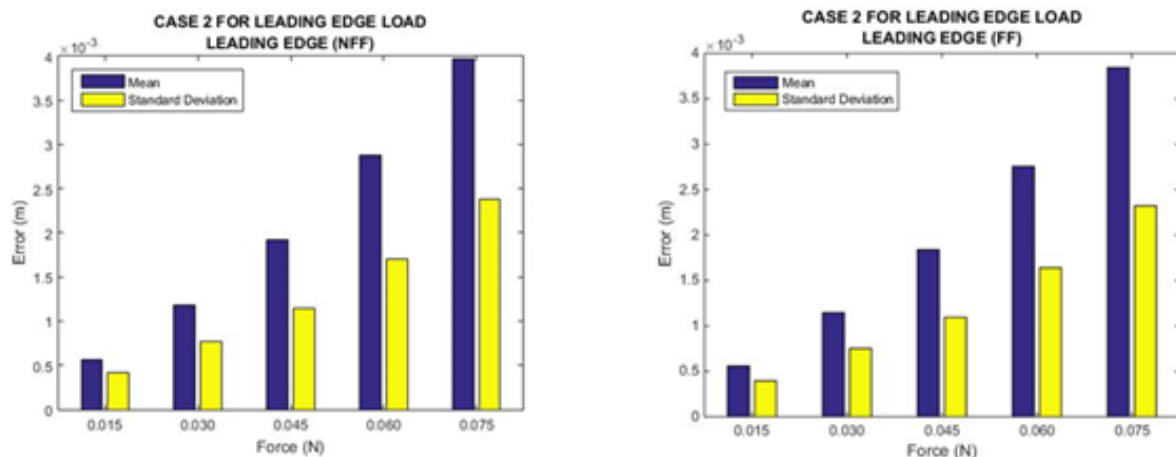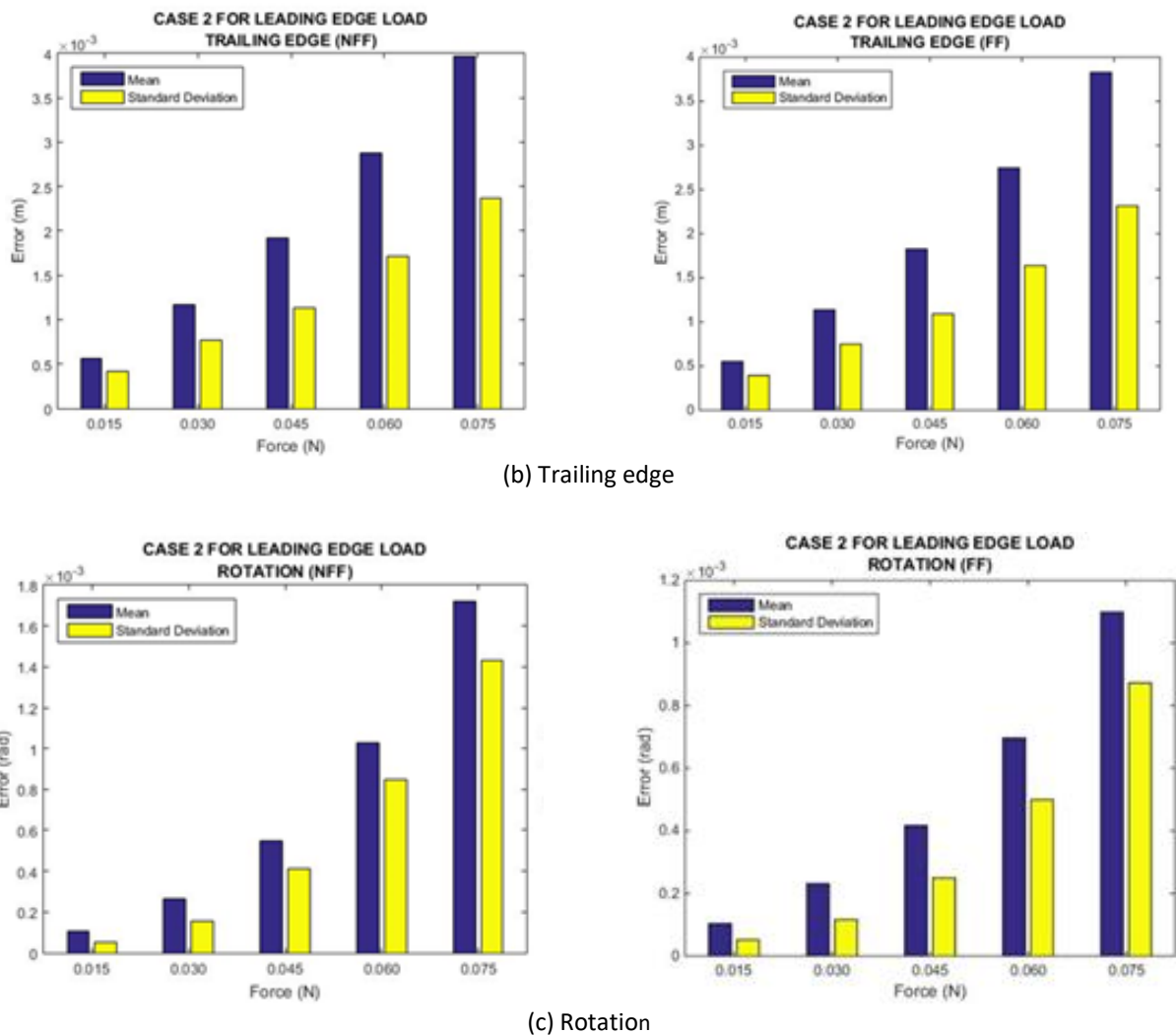
Fig. 11. Mean error and standard deviation of Case 2 for non-follower and follower forces for leading edge loading

3.5 Case 3 to Predict Deformations due to Uniform, Twist and Leading Edge Load

The NROM equations of Case 3 including all type of load to capture bending and rotational profile presented in Table 7.

Table 7
NROM equations

NROM equations	
Non-follower forces	$F_{B1} = 90.4\ P_{B1} + 64.91\ P_{B1}^2 + (3.78 \times 10^3)\ P_{B1}^3$
	$F_{T1} = 256100\ P_{T1} + (1.68 \times 10^8)\ P_{T1}^2 - (1.26 \times 10^{11})\ P_{T1}^3$
Follower forces	$F_{B1} = 90.4\ P_{B1} + 54.38\ P_{B1}^2 + (2.3 \times 10^3)\ P_{B1}^3$
	$F_{T1} = 256100\ P_{T1} + (1.53 \times 10^8)\ P_{T1}^2 - (1.17 \times 10^{11})\ P_{T1}^3$

3.5.1 NROM (case 3) to predict uniform loading

Figure 12 indicates the summary result of mean error and standard deviation for both non-follower and follower force effect for the NROM case 3 to predict uniform loading. Based on the results, the maximum mean error is found at the highest magnitude force with approximately

maximum mean error 4 mm for both cases. The NROM for case 3 which was developed with deformation for the three types of loading is able to predict the deformation of HAR wing plate model for uniform loading with significant accuracy.
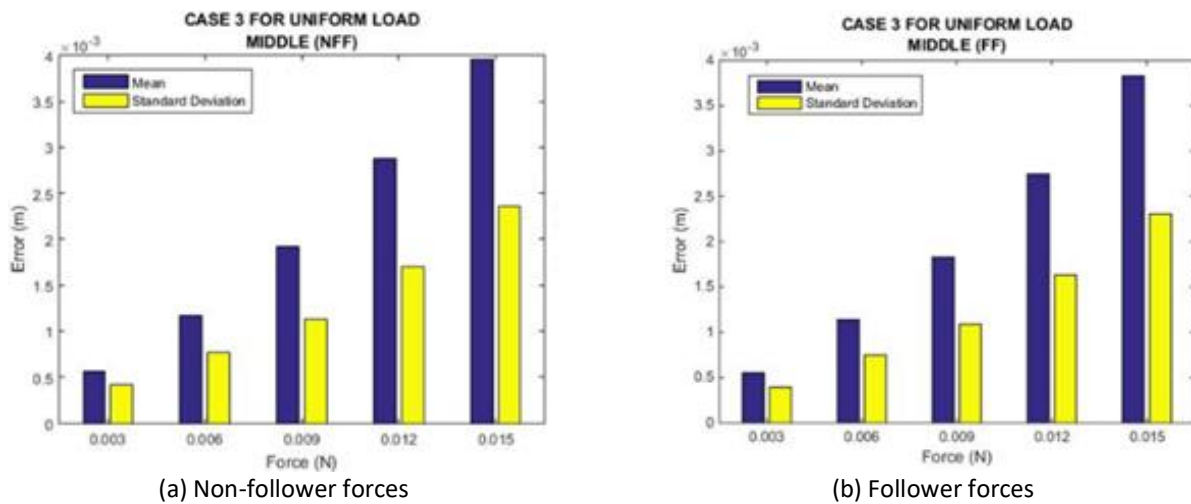
(a) Non-follower forces   (b) Follower forces

Fig. 12. Mean error and standard deviation of Case 3 for uniform loading

3.5.2 NROM (case 3) to predict twist loading

Figure 13 presents the summary result of mean error and standard deviation for the NROM case 3 to predict twist loading. Based on the results, the maximum mean error is found at the highest magnitude force for non-follower forces with a maximum error of approximately 0.06 rad while a maximum mean error for follower forces with a maximum mean error of 0.035 rad. For both cases, the mean error can consider significantly small. The NROM for case 3 can be considered effective, however the NROM for case 2 has more accuracy in the prediction of twist deformation. The inclusion of leading edge loading deformation in the NROM has a negative effect towards the prediction of twist loading deformation.
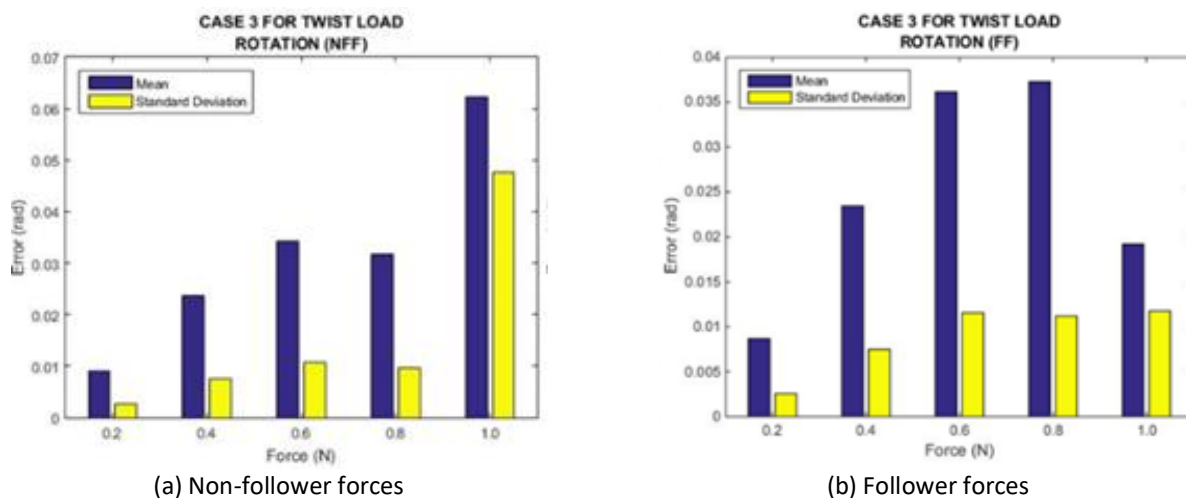
(a) Non-follower forces   (b) Follower forces

Fig. 13. Mean error and standard deviation of Case 3 for twist loading

3.5.3 NROM (case 3) to predict leading edge loading

Figure 14 presents the summary result of mean error and standard deviation to predict leading edge loading. Based on the results, for leading and trailing edge cases show that the maximum mean error is found at the highest magnitude force with approximately maximum mean error 4 mm for both cases. For rotation, a maximum mean error non-follower and follower forces are approximately 0.0015 rad and 0.0009 rad, respectively. The NROM developed for case 3 has slightly better accuracy in comparison to the prediction of NROM case 2 in prediction of the leading edge loading deformation.

(a) Leading edge

(b) Trailing edge

(c) Rotation
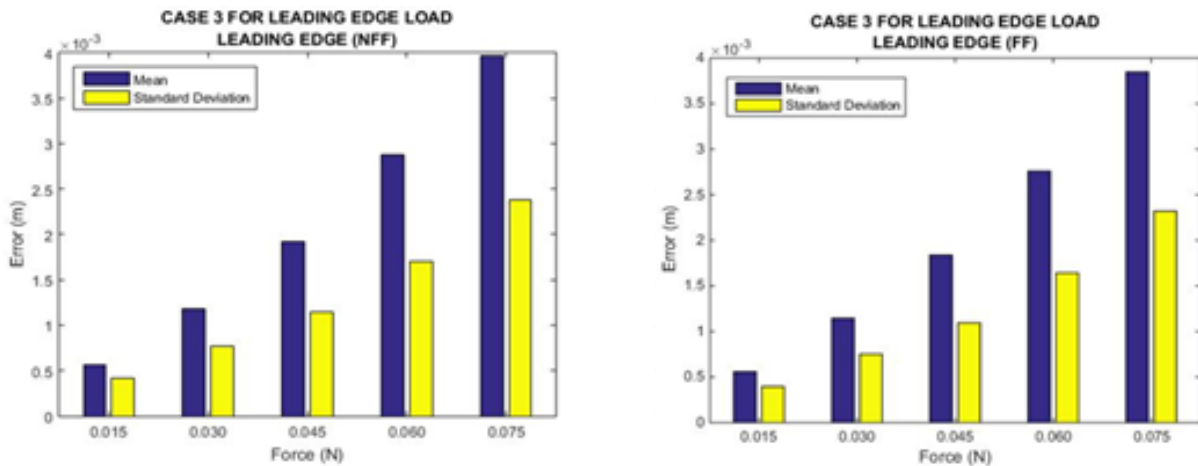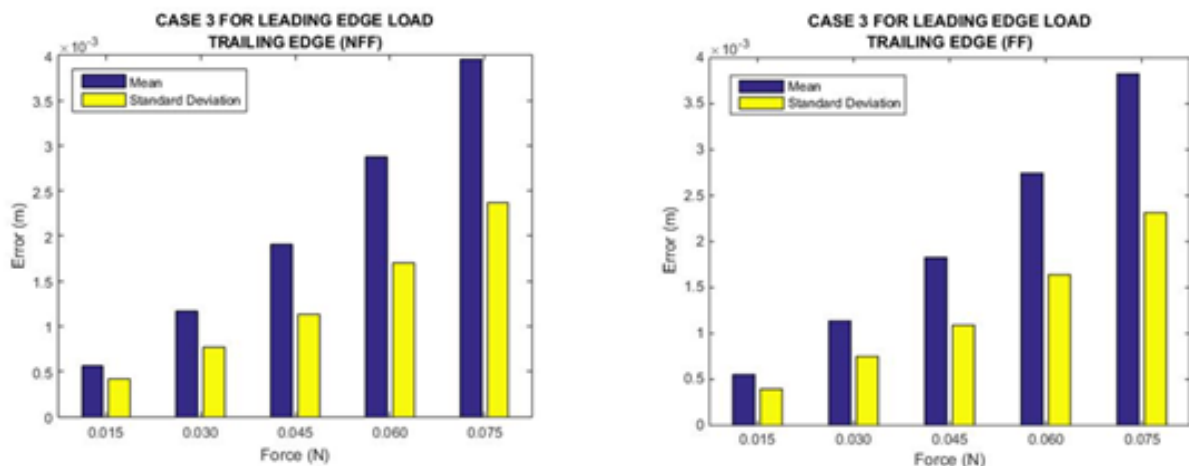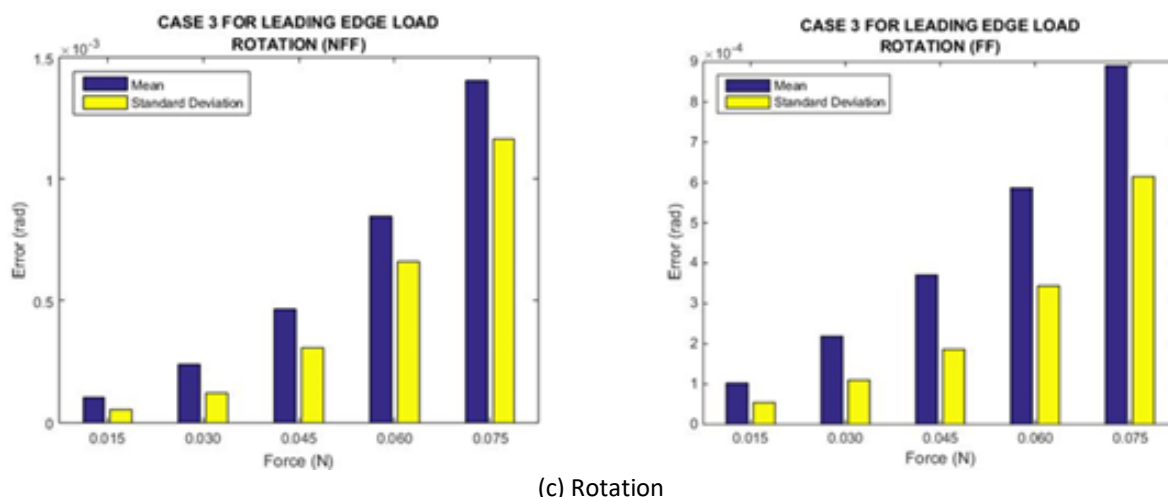
Fig. 14. Mean error and standard deviation of Case 3 for non-follower and follower forces for leading edge loading

4. Conclusions

The aim of this paper is to verify accuracy of development NROM via CMFE approach with the inclusion of the follower force effect on the HAR wing model with the conventional FEM of nonlinear static analysis. The main findings were as followed: (a) the result on nonlinear static analysis of HAR wing model based on NROM via CMFE exhibit a good agreement with the nonlinear static analysis using conventional FEM for all considered the load cases; especially in term of leading edge load case. In this study, leading edge load case replicate an actual aerodynamic load and represents simple aerostatic solution (b) the significant saving in term of computational time using NROM compare to the traditional method using FEM analysis and (c) follower forces inclusion shows larger displacement compared to non-follower forces and become more significant as the applied force increased. Even though the NROM via CMFE approach does sacrifice a certain degree of computational accuracy, but the solution is still an attractive option when compared with a conventional nonlinear static solution.

References
[1] Abbott, Ira H., and Albert E. Von Doenhoff. *Theory of wing sections: including a summary of airfoil data*. Courier Corporation, 2012.
[2] Afonso, Frederico, Gonçalo Leal, José Vale, Éder Oliveira, Fernando Lau, and Afzal Suleman. "LINEAR VS NON-LINEAR AEROELASTIC ANALYSIS OF HIGH ASPECT-RATIO WINGS." In *Congress of Numerical Methods in Engineering*, vol. 29. 2015.
[3] Smith, M., M. Patil, and D. Hodges. "CFD-based analysis of nonlinear aeroelastic behavior of high-aspect ratio wings." In *19th AIAA Applied Aerodynamics Conference*, p. 1582. 2001.
[4] Harmin, M. Y., and J. E. Cooper. "Aeroelastic behaviour of a wing including geometric nonlinearities." *The Aeronautical Journal* 115, no. 1174 (2011): 767-777.
[5] Tianxia, Song. "Nonlinear structure finite element computation." *University of Science & Technology Press, HuaZhong* (1996).
[6] Xie, Changchuan, Yi Liu, Chao Yang, and J. E. Cooper. "Geometrically nonlinear aeroelastic stability analysis and wind tunnel test validation of a very flexible wing." *Shock and Vibration* 2016 (2016): 1-17.

[7]   Salleh, Imran Mohd, Shamsul Sarip, Mohd Nabil Muhtazaruddin, and Mohamad Zaki Hassan. "Structural health monitoring (SHM) on high stress loading of wing bracket." *Journal of Advanced Research in Applied Mechanics* 27, no. 1 (2016): 16–22.
[8]   Chae, Seungmook. "Effect of follower forces on aeroelastic stability of flexible structures." PhD diss., Georgia Institute of Technology, 2004.
[9]   Tae H. Kim. "Follower-Force experiments with geometric nonlinear coupling for analytical validation." PhD diss., Air Force Institute Technolgy, 2011.
[10]   Xie, Changchuan, Chao An, Yi Liu, and Chao Yang. "Static aeroelastic analysis including geometric nonlinearities based on reduced order model." *Chinese Journal of Aeronautics* 30, no. 2 (2017): 638-650.
[11]   Castellani, Michele, Jonathan E. Cooper, and Yves Lemmens. "Nonlinear static aeroelasticity of high aspect ratio wing aircraft by FEM and multibody methods." In *15th Dynamics Specialists Conference*, p. 1573. 2016.
[12]   McEwan, M. I., Jan R. Wright, Jonathan E. Cooper, and Andrew Yee Tak Leung. "A combined modal/finite element analysis technique for the dynamic response of a non-linear beam to harmonic excitation." *Journal of Sound and Vibration* 243, no. 4 (2001): 601-624.
[13]   Thinesh, C., and Y Harmin, M. "Nonlinear reduced order model of high aspect ratio rectangular wing plate." *International Journal of Engineering & Technology* 7, no. 4.13 (2018): 195-201.
[14]   Rosly, N. A., and M. Y. Harmin. "Finite element analysis of high aspect ratio wind tunnel wing model: A parametric study." In *Materials Science and Engineering Conference Series* 270, no. 1 (2017): 012023.
[15]   MSC Software. Bulk Data Entry Descriptions. In MSC Nastran Quick Reference Guide. (2013).